Nuclear Instruments and Methods in Physics Research B 581 (2026) 166346

Contents lists available at ScienceDirect

Nuclear Inst. and Methods in Physics Research, B

journal homepage: www.elsevier.com/locate/nimb

Proton irradiation of Antarctic cryptoendolithic communities for the CRYPTOMARS project☆

G. Bazzano [a,*], A. Ampollini [a], M.D. Astorino [a], A. Doria [a], F. Fortini [a], P. Nenzi [a], E. Nichelatti [b], E. Pavoni [a], G. Picardi [a], M. Piccinini [a], V. Surrenti [a], E. Trinca [a], M.A. Vincenti [a], L. Selbmann [c], C. Del Franco [c], A. Cemmi [b], I. Di Sarcina [b], S. Bollanti [a], D. Murra [a], C. Donati [d], P. Franceschi [d], M. Garcia-Aloy [d], C. Ronsivalle [a]

[a] Nuclear Dept, ENEA C.R. Frascati, Via Enrico Fermi 45, 00044 Frascati, Roma, Italy
[b] Nuclear Dept, ENEA C.R. Casaccia, Via Anguillarese 301, Roma, 00123, Italy
[c] Department of Ecological and Biological Sciences, University of Tuscia, Viterbo, Italy
[d] Research and Innovation Centre, Fondazione Edmund Mach, San Michele all'Adige, Italy

ARTICLE INFO

Keywords:
Proton beam irradiation
Low dose irradiation
Astrobiology
Lithium fluoride

ABSTRACT

An irradiation campaign for astrobiology research was carried out at ENEA Frascati Research Center within the CRYPTOMARS project. The aim of the campaign was to characterize the responses of microbial communities colonizing Antarctic sandstone to ionizing radiation, at a dose level informed by the Martian surface environment. Proton irradiation is one of several stress factors applied separately within the project.

The experiment was carried out at the TOP-IMPLART proton accelerator, a technology demonstrator of a fully linear protontherapy machine with 71 MeV maximum beam energy.

Challenges of this experiment lie mainly in the realization of a tailored accelerator set-up, allowing a reproducible and controlled delivery of very low doses (down to 50 mGy with irradiation times of at least half an hour) to 70 Antarctic rock samples.

This was achieved thanks to the capabilities of the accelerator to be operated at currents down to 1 μA and perform dose-driven irradiations. To further reduce the dose-rate, the samples were irradiated in a specifically designed support in order to be exposed to the beam halo only. Doses down to 65 μGy per pulse were achieved with this set-up.

We report the experimental set-up design, the dosimetric characterization and the beam monitoring of the campaign; the biological analyses are ongoing and will be reported separately.

1. Introduction

The CRYTPOMARS project, funded by the Italian Space Agency (ASI) and led by the department of Ecological and Biological Sciences of University of Tuscia (UniTus), is a multidisciplinary research project aimed at investigating, with a multi-omic approach, the mechanisms of resistance developed by microbial communities living in the airspaces of sedimentary rocks of Continental Antarctica. These communities, exploiting the refuge provided by the rock, survive in an environment referred to as "Martian analogue on Earth" [1].

Investigation of their metabolic properties is conducted after exposing colonized samples of Antarctic rocks, separately, to different stress factors representative of the Martian environment, such as thermal and hydration/dehydration cycles, UV and ionizing radiation. The dose levels and dose rates for each treatment were selected with the aim of mimicking, as closely as possible, the chronic exposure conditions on the planet Mars, based on literature evidence [2].

The radiation environment on Mars surface is much harsher than the one experienced on Earth, due to the lack of magnetic shielding and an atmosphere of comparable thickness, and very different in radiation composition and spectra. Protons with energies ranging from tens of MeV to tens of GeV are predominant in the space radiation composition,

☆ This article is part of a special issue entitled: '2025 Proceedings ECAART15' published in Nuclear Inst. and Methods in Physics Research, B.

* Corresponding author.
E-mail address: giulia.bazzano@enea.it (G. Bazzano).

https://doi.org/10.1016/j.nimb.2026.166346
Received 27 January 2026; Received in revised form 9 September 2026; Accepted 10 October 2026
Available online 13 October 2026
0168-583X/© 2026 The Authors. Published by Elsevier B.V. This is an open access article under the CC BY license (http://creativecommons.org/licenses/by/4.0/).

especially in the Galactic Cosmic Rays (GCR) and the Solar Particle Events (SPE). Energetic protons, above ≈150 MeV before atmospheric transport, penetrate the Mars atmosphere, whose column depth at Gale crater is of the order of 20 g cm^{-2}, and are therefore present on the surface, together with secondary radiation such as neutrons and photons produced by their interaction with the Martian soil [3,4]. For comparison, the terrestrial atmospheric column at sea level is about 1030 g cm^{-2}, and the ground-level field is dominated by secondary cascades [5]. Protons of a few tens of MeV, such as those used here, reach the Martian surface mainly as secondaries or degraded primaries [6].

Two types of ionizing radiation stresses were selected within the CRYPTOMARS project: protons and gamma rays. Both were provided by ENEA facilities, such as the TOP-IMPLART proton linear accelerator in ENEA Frascati Research Center [7,8] and the CALLIOPE Co^{60} gamma source in ENEA Casaccia Research Center [9]. The two qualities were included to look for distinguishable signatures in the biological and multi-omic response; each exposure is characterized here by absorbed dose, dose rate, energy, LET and fluence.

Most climatic and radiative stresses, such as thermal cycles and UV exposure, within the CRYPTOMARS project targeted a 21-day worth period. Available experimental data from literature is provided by the Radiation Assessment Detector (RAD) from the Curiosity mission [4]. The RAD detector measured the Mars surface GCR dose contribution for a 300-day period at Gale crater. The average dose rate in tissue-like material resulted in 0.21 ± 0.04 mGy/day and a total dose of 76 mGy/year, that is 4.4 mGy for 21-day period.

However, two factors have been considered in the definition of the target dose for the proton irradiation campaign. First, Curiosity data were taken at a solar maximum, which modulates the GCR fluxes producing a dose rate minimum; RAD subsequently measured an increase of about 50% in the surface dose rate towards solar minimum [10]. Secondly, such a low dose poses significant challenges in accurate dose delivery to facilities designed to provide doses and dose rates typical of clinical applications. As a comparison, low dose proton irradiation studies for radiobiology experiments, aimed either at cancer treatment research [11] and space environment effect on human or animal tissue [12–14], delivered minimum doses in the 100 – 200 mGy range. Additionally, radiation resistance to high doses (> 1 kGy) of specific members of the cryptoendolithic communities is already established [15]. Taking these factors into account, a 10 × factor was applied to the target dose which was set at 50 mGy.

Whereas the Co-60 irradiation allows chronic exposure over a 21-day period, proton irradiation had to be compacted due to limitations on beam time and beam irradiation area: the required dose was thus delivered in sessions of approximately 30 to 50 min.

In this paper, we report the beam delivery method and the dosimetry of the proton irradiation campaign at the TOP-IMPLART accelerator, in the detail required for it to serve as the methodological reference for the biological work. The post-irradiation viability, metagenomic, metabolomic and lipidomic analyses are ongoing and will be reported in a dedicated astrobiology publication. A further, smaller set of rock samples was irradiated at high dose within the same campaign, for proton attenuation measurements and for the characterization of the microbial communities before and after irradiation by optical and spectroscopic techniques; those exposures are not covered here.

2. The beam delivery system

The TOP-IMPLART accelerator at ENEA Frascati Research Center has been developed as a technology demonstrator of a pulsed fully linear machine for protontherapy. It is equipped with two extraction beamlines: a low energy (1–6 MeV) vertical beamline and a high energy (up to 71 MeV) horizontal beamline. The latter was used for the CRYPTOMARS project irradiation campaign.

On the horizontal extraction beamline [16] the beam is delivered in 2.4 μs-long pulses at a repetition frequency of 25 Hz. Before extraction in air, the beam is transported in a short pipe equipped with an AC Current Transformer for non-destructive online beam monitoring. The maximum proton current is 20 μA and can be reduced acting on the voltage of an Einzel lens, placed at the proton source level, down to a current of 1 μA, the minimum that can be reliably detected by the AC Current Transformer.

The beam exits the accelerator through a 25 μm titanium window. It is then transported in air for 13 cm before entering a 1.7 m long extraction pipe filled with atmospheric pressure helium and equipped with a pair of scanning magnets. The pipe and the scanning magnets are designed to deliver the proton beam on a 10 x 10 cm^2 surface area at the nominal target position placed at 2.7 m downstream the titanium exit window (63 cm after the exit of the extraction pipe). In the air gap between the two pipes, an integral ionization chamber acts as an extracted beam Intensity Monitor, allowing dose-driven irradiation. The output of such Intensity Monitor chamber is read in an arbitrary unit called "Monitor Unit" (MU) that can be correlated to a dose value imparted at a given irradiation position. This is achieved by cross-calibrating the Intensity Monitor readings with a dose value obtained from a dosimeter placed at the desired irradiation position. In this way, dose driven irradiation can be achieved: the accelerator control automatically shuts off the beam once a preset amount of MUs are extracted.

Due to interaction with multiple materials, the maximum beam energy of 71 MeV reduces to 69.3 MeV at 63 cm from the exit of the extraction pipe [17,18] where the target is placed. The measured energy is consistent with SRIM [19] computation which takes into account the beam energy distribution at the exit of the accelerator, given by the LINAC code [20] and the materials that constitute the beam transport line. The beam, of gaussian transverse distribution, here has a round spot with a FWHM of 25 mm.

The samples of the CRYPTOMARS proton campaign are irregularly shaped fragments of Antarctic sandstone collected at seven different sites. For each site, ten fragments were exposed: five colonized, that is containing cryptoendolithic communities, and five uncolonized, without such colonies, for a total of 70 rocks. Colonized and uncolonized samples differ in their biological content and not in their treatment: both were exposed to the same single dose condition with identical beam settings. No sham-irradiated group was included.

The cryptoendolithic samples are placed for exposure to stress factors in multiwell plates of external dimensions 8 × 12 cm^2, each containing twelve 1.5 cm wide, 1 cm deep cylindrical housings (see Fig. 1). The size of such a plate is compatible with active scanning beam delivery, covering at least nine samples. This irradiation scheme would have the advantage of providing high beam transverse homogeneity. However, even at a reduced proton current of 1 μA, with the beam distributed over the 10 x 10 cm^2 scanned field at the full 25 Hz repetition rate, the minimum achievable flux is of the order of 3×10^6 protons cm^{-2} s^{-1} which, for a 69 MeV proton beam with stopping power 9.66 MeV cm^2 g^{-1} [21], corresponding to a water-equivalent LET of approximately 0.97 keV/μm, corresponds to an entrance dose-rate of nearly 5 mGy/s, too high for the presented application. This is a rapid estimate based on the nominal current and scanned field.

For this reason, a passively scattered, non-scanned halo irradiation approach was instead chosen, schematically depicted in Fig. 2. The proton beam exiting the accelerator is diffused with a 120 μm-thick lead scattering foil placed in air between the ionization chamber Intensity Monitor and the entrance of the extraction pipe. The proton beam propagates and expands in the helium filled extraction pipe: the resulting widened beam has a diameter of 14 cm at the nominal target. To further reduce the dose rate on the cryptoendolithic targets, the samples are arranged as depicted in the inset of Fig. 2, to intercept only the beam halo. Working in the halo rather than on the beam axis reduces the dose rate at the sample positions by a factor of about five with respect to the axis value, at the cost of a radial non-uniformity that is characterized below. This reduction alone is not sufficient to reach the required irradiation time, and a second, independent reduction is

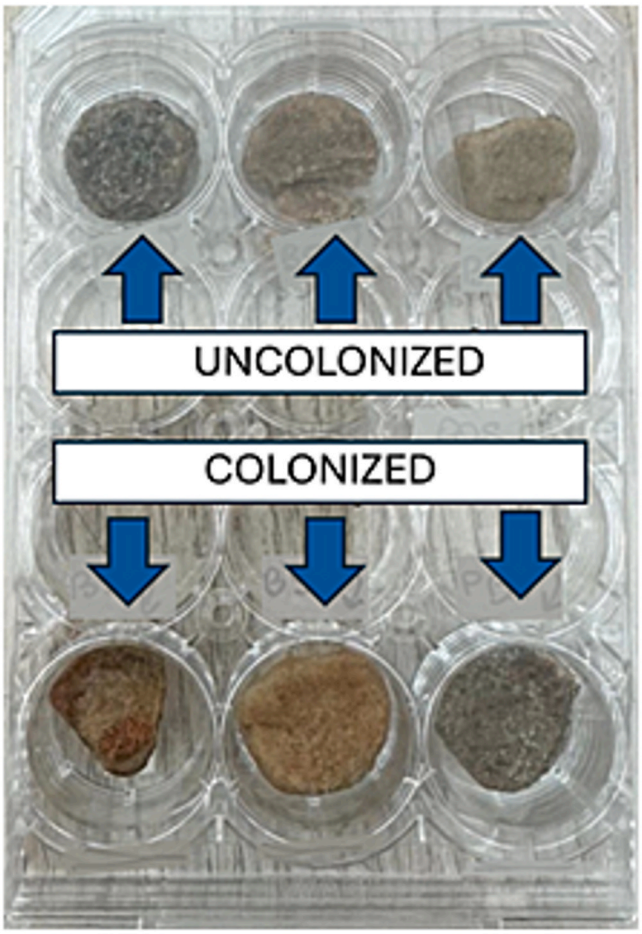


Fig. 1. Colonized (bottom) and uncolonized (top) Antarctic rock samples housed in multiwell plate; the position has been set to ensure a uniform exposure to the proton beam. Colonized samples contain cryptoendolithic communities, uncolonized ones do not; both types were irradiated with identical beam settings.

obtained by lowering the beam duty cycle, as described later in this section. This arrangement consists of three multiwell plates positioned at 120 degrees with a total of 9 rock samples to be irradiated simultaneously. In each plate, only 6 of the twelve wells are filled (highlighted in green and yellow), so that two sets of three samples per plate can be brought into the halo in turn: the green ones are exposed in the first orientation, and after one irradiation run the plates are reversed so that the yellow ones are brought into the same geometry. The two colours therefore identify successive irradiation orientations, and each sample receives one intended exposure.

A dedicated holder was designed, and realized in house with 3D printing technique, to ensure reproducible and fast positioning of the multiwell plates (see Fig. 3). Each group of 3 plates remains in the bunker for approximately 2 h for the whole irradiation process, including two irradiation runs of 30 to 50 min and the plate reversal, with cool air cycling in the sample holder at approximately 16 °C. The temperature of the rocks was not monitored directly; given the limited residence time, the set-up was considered adequate by the biological team to avoid thermal stress to the cryptoendolithic communities.

3. Dosimetric characterization

The preliminary characterization of the beam on the irradiation target was aimed at achieving the best dose uniformity possible on the samples and at defining the machine operating conditions required to deliver the dose specified for the experiment.

The target rocks used in the experiment exhibit significant variability and irregularity in shape, as well as in structure and density, as they consist of sedimentary rocks collected from different regions of Antarctica and characterized by different degrees of porosity. The organisms colonizing these rocks are confined to the outermost millimeters beneath the surface, but their exact depth and distribution within each rock were not mapped before irradiation. The quantity prescribed for the experiment was the absorbed dose at the sample entrance surface, with no internal depth-dose distribution specified.

The cryptoendolithic colonies were irradiated at the maximum available proton beam energy in order to minimize the entrance LET and to maximize longitudinal dose homogeneity over the potentially colonized layer, ensuring that the Bragg peak occurs well beyond it. Since no material model representative of the irradiated rock types was available for dose-deposition simulations, a conservative estimate of longitudinal dose uniformity was adopted.

The average energy of protons incident on the samples was evaluated using SRIM, accounting not only for attenuation caused by the standard materials of the beamline but also by the diffuser (Pb, 120 μm) and the multiwell-plate lid (polystyrene, 1 mm). The resulting proton energy is 68.1 MeV. In the absence of a precise match for the target material in the SRIM library, the material “concrete” was used as an approximation: being a heterogeneous silicate with a density (2.3 g cm^{-3}) close to that of a porous sandstone, it is a better approximation than pure quartz. In any case, silicate materials of this kind have very similar mass stopping powers at this energy, and the Bragg peak lies far beyond the region of interest, so the choice has little influence on the result. The simulation predicts a 14% increase in LET at a depth of 5 mm compared to the surface value, 5 mm being a plausible upper bound for the colonized layer; the local dose varies by a comparable amount.

The dosimetric devices employed for the experiment are radiochromic films and lithium fluoride (LiF) crystals, usually employed at the TOP-IMPLAT accelerator [22–25]. The two systems had different purposes: the films provided rapid two-dimensional information during the iterative optimization of the scattering geometry, holder position and halo distribution, while the calibrated LiF crystals provided the final dose characterization and the relation between Monitor Units and absorbed dose at the sample positions. Only the LiF measurements were used to assign the dose delivered to the samples. However, the detection limits of these sensors do not allow for direct measurements at the target dose values required for this experiment (< 0.1 Gy). Therefore, the dose evaluation was carried out in two steps: first, the measurement of the ratio between the dose on the beam axis and the dose in the beam halo at the position of the multiwells; second, the calibration between the dose on the beam axis and the beam intensity monitor. This procedure enables a correlation between the extracted beam intensity, expressed in MU, and the dose delivered to the multiwells, thus allowing irradiation at predefined dose levels.

The ratio between the on-axis dose and the halo dose is mainly dependent on the scattering of the beam due to interaction with the various materials along the extraction line and, in particular, with the lead diffuser. Conversely, it does not depend on the beam intensity. The measurement of the dose ratio between the beam center and the multiwells was therefore initially performed under conditions of relatively high dose and high dose rate (with a proton current per pulse of approximately 5 μA), compared to the target experimental conditions, and subsequently repeated to verify the stability of this ratio at the minimum achievable dose rate (proton current per pulse of approximately 1 μA).

Radiochromic films were used for a preliminary assessment of the dose ratio stability as a function of dose rate. For each measurement, a film sheet was placed on top of the lids of three empty multiwell plates in order to capture the full beam spot. The radiochromic films were analyzed using an Epson Expression 11000XL flatbed scanner in transmission mode, with no color correction applied, at a resolution of 400

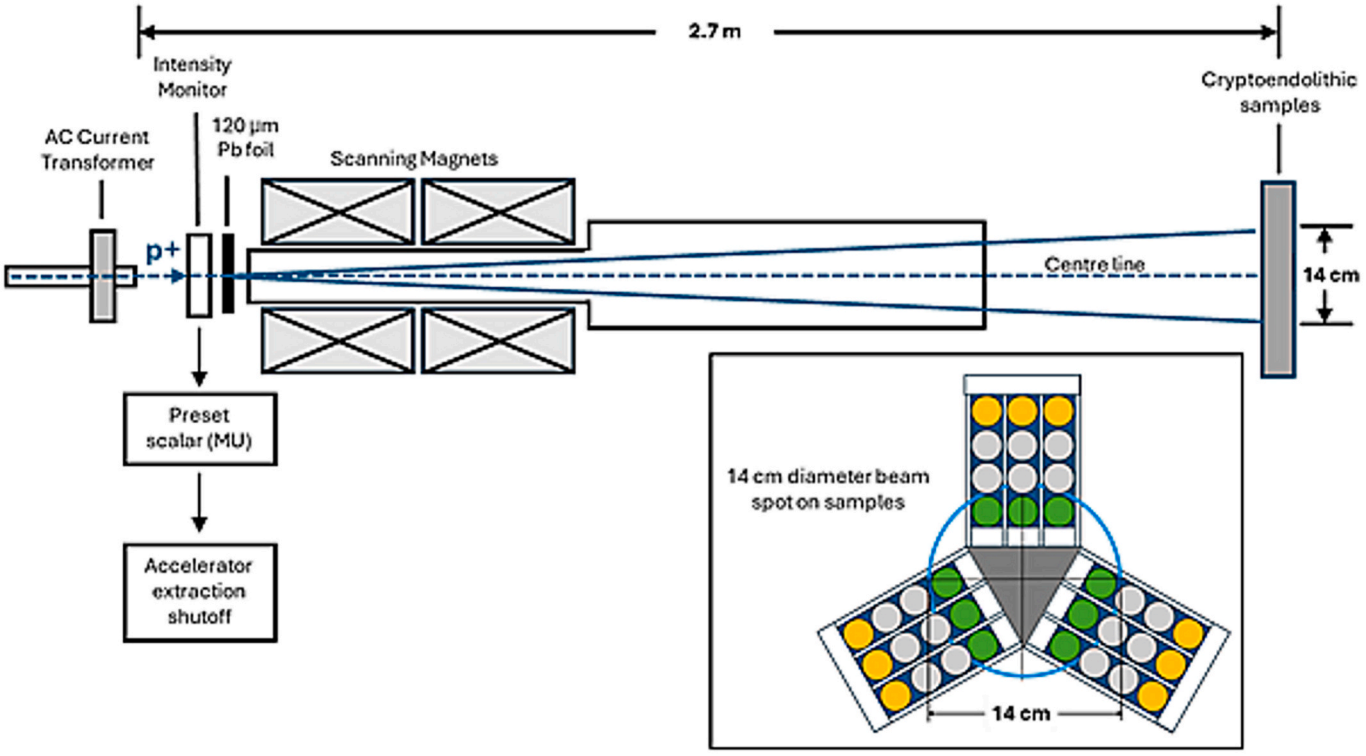


Fig. 2. Schematic representation of the beam delivery scheme and layout of the samples.



Fig. 3. Multiwell plates irradiation holder positioned at the end of the beam pipe at the TOP-IMPLART accelerator.

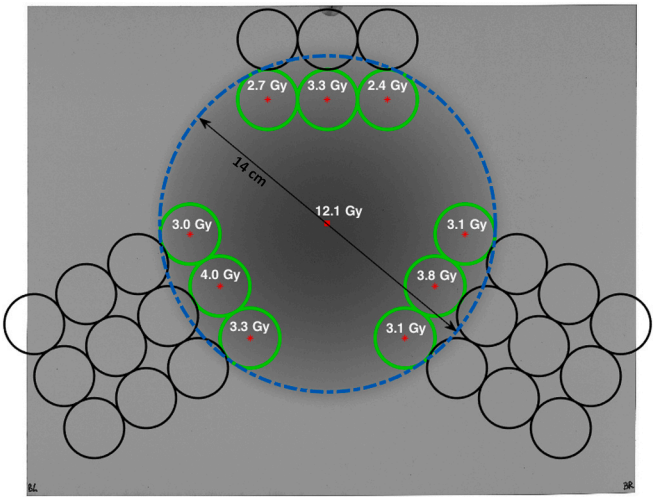


Fig. 4. Representative EBT3 dose map used during set-up optimization, with the multiwell geometry superimposed; the selected wells intercept the useful off-axis halo, while the wells not exposed in that plate orientation show no measurable dose within the practical range of the film screening method.

dpi and a 24-bit color depth. The digitized images were then converted to grayscale and analyzed to extract dose values in selected regions of interest (ROIs) through a MATLAB script, based on the general calibration equation described in [26,27]. The general calibration equation offers a fast if rough estimation of dose, typically with an accuracy of ± 5%. The films were read shortly after irradiation rather than after the standard 24 h stabilization interval: the optimization was iterative and had to converge within the available beam time, and in our experience this is also the condition under which the general calibration equation agrees best with calibrated dosimeters. A representative dose map, with the multiwell geometry superimposed, is shown in Fig. 4.

Following the preliminary evaluation with radiochromic films, measurements were carried out using LiF crystal dosimeters, calibrated for absorbed dose in water with a Co^{60} source at the Italian National Institute of Metrology for ionizing radiation (INMRI) [28]. For each dosimetric session, ten crystals with dimensions of 5 × 5 mm^2 and a thickness of 1 mm were used, arranged as follows: one positioned at the center of the sample holder and nine placed inside the wells of the multiwell plates exposed to the beam halo. Measurements were performed at high dose rate and high total dose and subsequently repeated at the minimum dose rate with reduced total dose value; all calibration exposures were carried out at the full 25 Hz repetition rate, without duty cycle reduction. The estimated uncertainty for these measurements is ± 0.1 Gy, the typical residual of the calibration fit.

Table 1 summarize the main results of the dosimetric measurements of dose on the beam axis performed with EBT3 films and LiF crystals at two different proton intensities. Since the total number of MU differs

Table 1
Summary of dose on axis measurement with EBT3 films and LiF crystals at two different proton beam intensities. MU/pulse is obtained as the ratio between the total delivered MU and the recorded number of pulses; the pulse-by-pulse values were not recorded for these sessions, so no standard deviation is quoted. Uncertainties on the measured doses are one standard deviation.

Detector	ACCT current	Average MU/pulse	Delivered MU	$Dose_{axis}$	$Dose_{axis}$/MU
	[μA]	[-]	[-]	[Gy]	[μGy]
EBT3	5	8.0	1.8×10^5	23.7 ± 1.2	132 ± 7
EBT3	1	3.2	1.2×10^5	12.1 ± 0.6	101 ± 5
LiF	5	7.7	1.8×10^5	22.8 ± 0.1	127 ± 1
LiF	1	3.0	5.0×10^4	5.4 ± 0.1	108 ± 2

between sessions, the delivered MU are reported alongside the measured dose, and the comparison between the two detectors concerns the dose per MU rather than the absolute dose. The measured dose and their uncertainties are converted into Dose per MU in the last column of Table 1. The lower dose per MU measured at 1 μA reflects recombination effects in the ionization chamber, whose response depends on the dose per pulse [29], so no current-independent MU-to-dose conversion was assumed and the calibration used for the biological irradiations is the one obtained at 1 μA, i.e. at the actual operating condition. The dose measurements on the beam axis position obtained with LiF crystals are in agreement with the EBT3 films readings within the expected ± 5% accuracy; doses on the multiwell positions show instead greater discrepancies, up to ± 10%. This result is acceptable given the fact that the multiwell measurements are not taken in the same position (before the lid for the gafchromic and inside the well for the LiF detectors).

Fig. 5 summarizes the results of the measurement of ratio of dose at samples position and dose on-axis. The LiF measurements support the assumption that the dose ratio between the beam center and the halo is essentially independent of the beam intensity, the mean ratio over the nine positions being 0.21 at 5 μA and 0.20 at 1 μA. The measurements highlighted a dose variability among the individual wells due to the radial inhomogeneity of the beam halo: in particular, the three central wells receive a dose about 26% higher than the mean over the nine positions, while the six lateral ones receive about 13% less. The same pattern is found in both LiF measurements, the mean values of the two subgroups agreeing within two standard deviations at the two beam intensities; the samples were therefore grouped operationally into a central and a lateral set, and a nominal dose was assigned to each group. The position of each sample is retained in the irradiation records.

For the experimental campaign, only measurements obtained with calibrated LiF detectors were considered: the average ratio on all samples is 0.20, the ratio for the central wells is 0.25 and the ratio for the lateral wells is 0.17; the Dose on axis per MU at low current is D_{axis}/MU = 108 ± 2 μGy/MU. At 3 MU/pulse, the dose on axis per pulse was 324 μGy, corresponding to an average dose per pulse on the samples of approximately 65 μGy, 82 μGy in the central wells and 56 μGy in the lateral ones.

The target MU value for the irradiation of the cryptoendolithic samples was set to 2500: this corresponds to nominal entrance doses of 68 mGy in the three central wells and 47 mGy in the six lateral ones, and to a mean of 54 mGy over the nine positions.

At a pulse repetition frequency of 25 Hz and a rate of 3 MU/pulse, the 2500 MU irradiation would normally take about 30 s. To reach the desired irradiation duration of at least 30 min, the control of the beam veto was reprogrammed to allow not only the automatic shut-off of the irradiation once the preset number of MUs are delivered, but to also allow a reduced beam duty cycle. It was obtained by allowing the machine operator to programmatically control beam on and beam off periods of time. For the CRYPTOMARS irradiation it consisted in beam on periods of 1 s followed by 55 s beam off periods, resulting in an effective duty cycle of ≈ 1.8%.

The resulting operating conditions and the derived quantities at the sample positions are summarized in Table 2. Fluence values are obtained from the absorbed dose using the stopping power quoted above [21] and are therefore derived, not directly measured quantities.

The measured on-axis dose rate of 8.1 mGy/s is of the same order as the estimate given above for the active scanning option and, like it, too high for this experiment: the halo geometry and the reduced duty cycle together lower the mean dose rate at the sample positions by a factor of approximately 280 with respect to the on-axis beam-on value.

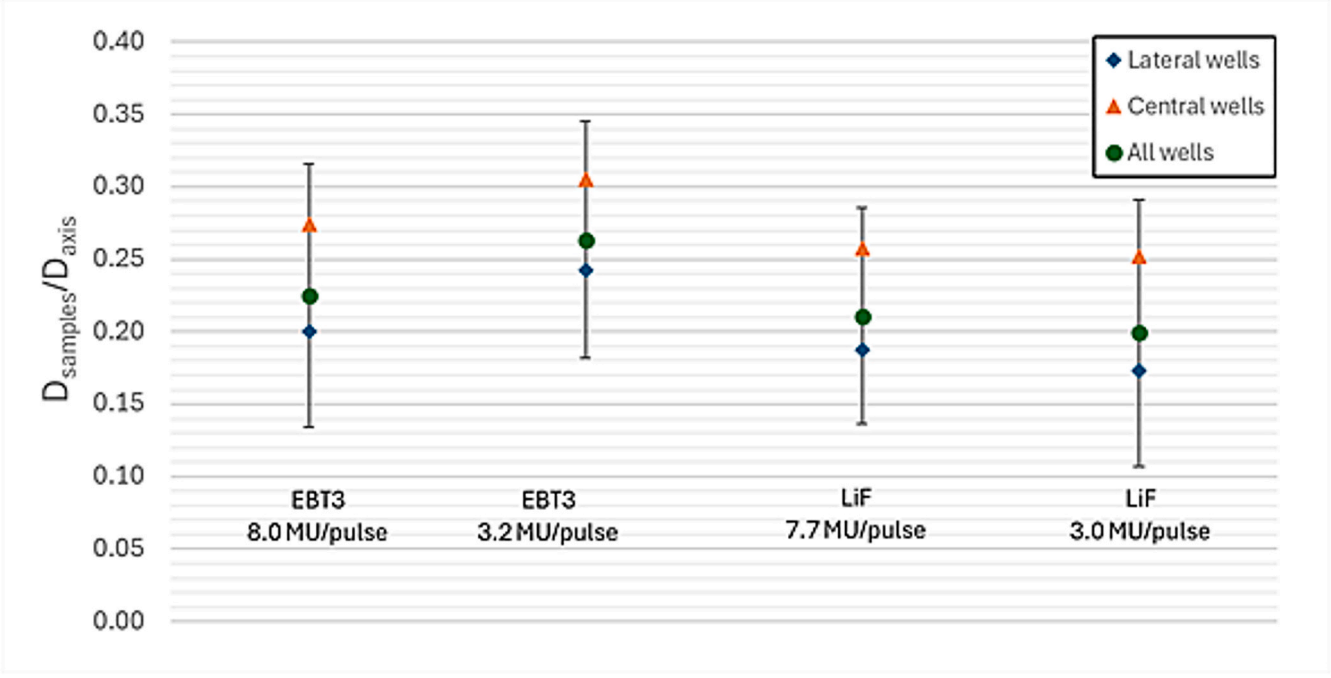


Fig. 5. Summary of measurement of ratio of dose at samples position and dose on-axis; ratios are shown as average on all wells with 2 standard deviations error bars; average values for the central and lateral wells subgroups are highlighted.

Table 2
Final operating conditions of the biological irradiations and derived quantities at the sample positions.

Parameter	Typical value
ACCT current	≈ 1 μA
Pulse structure	2.4 μs at 25 Hz
Nominal intensity	≈ 3 MU/pulse
Macro-cycle / duty cycle	1 s on + 55 s off / ≈ 1.8%
Dose per pulse, on axis	324 μGy
Mean dose per pulse, samples	65 μGy
Dose rate on axis, beam on	8.1 mGy/s
Mean dose rate on samples, beam on	1.6 mGy/s
Mean dose rate on samples, macro-cycle average	29 μGy/s
Mean flux on samples, beam on	1.0×10^6p $cm^{-2}s^{-1}$
Mean flux on samples, macro-cycle average	1.9×10^4p $cm^{-2}s^{-1}$
Total fluence on samples, 2500 MU	3.5×10^7p cm^{-2}

The uncertainty on the dose assigned to the samples was evaluated as follows, all values being quoted at two standard deviations. Since the ratios measured at the two beam intensities agree, those obtained at 1 μA, in the actual irradiation condition, were adopted. The dominant term is their spread among the wells of each group, ± 0.05 for both the central and the lateral positions; the ± 0.1 Gy resolution of the individual LiF readings is contained in this spread and is not counted separately. Adding in quadrature the MU-to-dose calibration, which amounts to 4%, the nominal entrance doses are 68 ± 12 mGy for the central and 47 ± 14 mGy for the lateral positions.

4. Irradiation dosimetry results

The 70 samples were irradiated in two days, divided in 8 irradiation runs of approximately 30 min each, over the 72 positions available in the eight runs, the two remaining positions being left unloaded. Plate number, side, irradiated row, sample identifiers, delivered MU and duration were logged for each run, so that every sample can be traced to its irradiation position and hence to its nominal dose. A summary of the recorded beam parameters is reported in Table 3.

Although some variability of the instantaneous dose rate within a single irradiation session was observed—quantified as the standard deviation of the MU/pulse value over the irradiation time—the average dose rate, expressed as the mean MU/pulse, remained substantially stable across the eight irradiation sessions. The maximum deviation of this parameter was within ± 3%. This matters because the response of the monitor chamber depends on the dose per pulse: the MU-to-dose conversion holds for a given intensity regime, and the campaign remained close to the 3 MU/pulse at which the calibration of Table 1 was obtained. The irradiation time was typically around 35 min, with the exception of irradiation no. 5, which lasted nearly 50 min because of a beam interruption; since the irradiation terminates on the integrated MU count, the delivered dose is unaffected and only the average dose rate is lower. The delivered MU agree with the 2500 MU target within 0.2% in all runs, so the delivery conditions established during the preliminary dosimetric characterization (average 3 MU/pulse, total of 2500 MU, and exposure duration ≈ 30 min) were fulfilled for all eight irradiations of the biological samples.

As further confirmation of the reproducibility of the defined setup, the total dose measured by the centrally placed GAF EBT3 film during the first four and the subsequent four irradiations was consistent with expectations from the preliminary dosimetric tests, yielding 1.00 Gy (total dose of the first four sessions – day 1) and 1.07 Gy (total dose of the second four sessions – day 2) against an expected on-axis value of 1.08 Gy for four runs. These values correspond to an average dose to the samples of 50 mGy and 53 mGy for the sessions carried out on day 1 and day 2, respectively, compatible with expectation within the accuracy of the film screening method.

Table 3
Summary of dosimetric information for the irradiation runs on the samples.

Irradiation run nr	Delivered MU	Irradiation duration	MU/ pulse average	MU/ pulse st dev
	[-]	[min]	[-]	[-]
1	2502	33	2.79	0.54
2	2502	34	2.84	0.53
3	2502	37	2.85	0.69
4	2502	33	2.84	0.62
5	2502	48	2.67	0.61
6	2504	39	2.83	0.72
7	2500	34	2.78	0.83
8	2500	32	2.83	0.51

5. Conclusion

A dedicated proton beam delivery and dosimetric approach was successfully developed at the TOP-IMPLART accelerator to enable controlled irradiation of cryptoendolithic Antarctic rock samples at very low dose levels, compatible with Mars-analogue conditions. By combining beam diffusion, halo irradiation geometry, dose-driven control integrated into the accelerator system and a reduced duty cycle, nominal entrance doses of 68 ± 12 mGy in the central and 47 ± 14 mGy in the lateral positions, two standard deviations, with a mean of 54 mGy over the nine positions, were reproducibly delivered over irradiation times of 30 to 50 min to 70 samples. The dosimetric characterization, based on radiochromic films and LiF detectors, demonstrated stable dose ratios between beam axis and halo and a position-dependent dose distribution among the samples, each of which is traceable to its irradiation position. These results show that a clinical-oriented proton linac can be effectively adapted for very low-dose astrobiology experiments, with quantified and reproducible dose control.

Declaration of competing interest

The authors declare that they have no known competing financial interests or personal relationships that could have appeared to influence the work reported in this paper.

Acknowledgments

This research has been carried on within the CRYPTOMARS project, funded by the Italian Space Agency (ASI) under the contract n. 2023-12-U.0, and the TOP-IMPLART (Oncological Therapy with Protons – Intensity Modulated Proton Linear Accelerator for Radiotherapy) project funded by Regione Lazio, Italy.

References

[1] S.C. Cary, I.R. McDonald, J.E. Barrett, D.A. Cowan, On the rocks: the microbiology of antarctic dry valley soils, Nat. Rev. Microbiol. 8 (2) (2010) 129–138, https://doi.org/10.1038/nrmicro2281.
[2] L. Selbmann, et al., The CRYPTOMARS project: a multi-omic approach for studying Antarctic cryptoendolithic communities as Martian-analog life-forms, Int. J. Astrobiol. 24 (2025) e17.
[3] F.A. Cucinotta, P.B. Saganti, J.W. Wilson, L.C. Simonsen, Model predictions and visualization of the particle flux on the surface of mars, J. Radiat. Res. 43 (S) (2002) S35–S39, https://doi.org/10.1269/jrr.43.S35.
[4] D.M. Hassler et al., Mars' surface radiation environment measured with the Mars Science Laboratory's Curiosity Rover, Science (1979)., vol. 343, no. 6169, Jan. 2014, doi: 10.1126/science.1244797.
[5] J.L. Barth, C.S. Dyer, E.G. Stassinopoulos, Space, atmospheric, and terrestrial radiation environments, IEEE Trans. Nucl. Sci. 50 (3) (2003) 466–482, https://doi.org/10.1109/TNS.2003.813131.
[6] B. Ehresmann, et al., Energetic particle radiation environment observed by RAD on the surface of mars during the september 2017 event, Geophys. Res. Lett. 45 (11) (2018) 5305–5311, https://doi.org/10.1029/2018GL077801.
[7] C. Ronsivalle, et al., The TOP-IMPLART project, Eur. Phys. J. plus 126 (7) (2011) 1–15, https://doi.org/10.1140/epjp/i2011-11068-x.

[8] P. Nenzi et al., Status of the top-implart proton linac, in Proceedings of LINAC2022, 31st Int. Linear Accel. Conf, Liverpool, UK, 2022, pp. 138–141. doi: doi:10.18429/JACoW-LINAC2022-MOPOGE02.
[9] S. Baccaro, A. Cemmi, I. Di Sarcina, G. Ferrara, Gamma irradiation Calliope facility at ENEA-Casaccia Research Centre (Rome, Italy), 2019.
[10] J. Guo, et al., Radiation environment for future human exploration on the surface of Mars: the current understanding based on MSL/RAD dose measurements, Astron. Astrophys. Rev. 29 (1) (2021) 8, https://doi.org/10.1007/s00159-021-00136-5.
[11] A. Almahwasi, Induced radioresistance in normal human cells following proton irradiation, Radiat. Phys. Chem. 237 (2025) 113136, https://doi.org/10.1016/j.radphyschem.2025.113136.
[12] J.H. Ware, et al., Effects of proton radiation dose, dose rate and dose fractionation on hematopoietic cells in mice, Radiat. Res. 174 (3) (2010) 325–330, https://doi.org/10.1667/RR1979.1.
[13] D.S. Gridley, et al., Low-dose, low-dose-rate proton radiation modulates CD4 $^{+}$ T cell gene expression, Int. J. Radiat Biol. 85 (3) (2009) 250–261, https://doi.org/10.1080/09553000902748609.
[14] B.P. Tseng, M.L. Lan, K.K. Tran, M.M. Acharya, E. Giedzinski, C.L. Limoli, Characterizing low dose and dose rate effects in rodent and human neural stem cells exposed to proton and gamma irradiation, Redox Biol. 1 (1) (2013) 153–162, https://doi.org/10.1016/j.redox.2013.01.008.
[15] L. Selbmann, et al., Resistance of an Antarctic cryptoendolithic black fungus to radiation gives new insights of astrobiological relevance, Fungal Biol. 122 (6) (2018) 546–554, https://doi.org/10.1016/j.funbio.2017.10.012.
[16] P. Nenzi et al., Commissioning of the 71 MeV beam delivery line of the TOP-IMPLART accelerator, in Proceedings of IBIC2025 - 14th International Beam Instrumentation Conference, Liverpool: JacoW, 2025.
[17] E. Nichelatti, et al., Spectral characterization of 63 and 71 MeV proton beams using localized random search fitting of radiophotoluminescent Bragg curves in lithium fluoride crystals, Nucl. Instrum. Methods Phys. Res. A 1088 (2026) 171481, https://doi.org/10.1016/j.nima.2026.171481.
[18] E. Nichelatti, et al., High-resolution diagnostics of the top-implart 71 MeV proton beam using photoluminescent color centers in LiF crystals, in: Proceedings of IBIC2025 - 14th International Beam Instrumentation Conference, 2025, https://doi.org/10.18429/JACoW-IBIC2025-MOPCO06.
[19] J.F. Ziegler, M.D. Ziegler, J.P. Biersack, SRIM – the stopping and range of ions in matter (2010), Nucl. Instrum. Methods Phys. Res. B 268 (11–12) (2010) 1818–1823, https://doi.org/10.1016/j.nimb.2010.02.091.
[20] K.R. Crandall, M. Weiss, LINAC code - TERA 94/34 ACC 20 (internal note), 1994.
[21] M.J. Berger, J.S. Coursey, M.A. Chang, ESTAR, PSTAR, and ASTAR: computer programs for calculating stopping- power and range tables for electrons, protons, and helium ion (version 1.2.3). Accessed: Jan. 13, 2022. [Online]. Available: https://www.nist.gov/pml/stopping-power-range-tables-electrons-protons-and-helium-ions.
[22] G. Bazzano et al., Beam characterization methods at the TOP-IMPLART proton linear accelerator: an application to space components qualification, in 2021 IEEE International Workshop on Metrology for AeroSpace, MetroAeroSpace 2021 - Proceedings, 2021. doi: 10.1109/MetroAeroSpace51421.2021.9511719.
[23] C. De Angelis, et al., The top-implart proton linear accelerator: interim characteristics of the 35 MeV beam, Radiat. Prot. Dosimetry 186 (1) (2019) 113–118, https://doi.org/10.1093/rpd/ncz142.
[24] E. Nichelatti, et al., Radiophotoluminescence of lithium fluoride detectors for beam diagnostics in a proton therapy linear accelerator. ICARST-2021, Second International Conference on Applications of Radiation Science and Technology, 2022.
[25] M. Piccinini, et al., Dynamic range and dose linearity of the radiophotoluminescence intensity in lithium fluoride crystals irradiated with 2.3 and 26 MeV protons, J. Lumin. 259 (2023), https://doi.org/10.1016/j.jlumin.2023.119833.
[26] L. Campajola, P. Casolaro, F. Di Capua, Absolute dose calibration of EBT3 Gafchromic films, J. Instrum. 12 (08) (2017) P08015–P, https://doi.org/10.1088/1748-0221/12/08/P08015.
[27] P. Casolaro, L. Campajola, F. Di Capua, The physics of radiochromic process: one calibration equation for all film types, J. Instrum. 14 (08) (2019) P08006–P, https://doi.org/10.1088/1748-0221/14/08/P08006.
[28] M. Piccinini, E. Nichelatti, M. Pimpinella, V. De Coste, R.M. Montereali, Dose response of visible color center radiophotoluminescence in lithium fluoride crystals irradiated with a reference 60Co gamma beam in the 1–20 Gy dose range, Radiat. Meas. 151 (2022) 106705, https://doi.org/10.1016/j.radmeas.2022.106705.
[29] A. Ampollini, et al., Recombination effects in the ionization chambers dose delivery monitor of the TOP-IMPLART proton beam, J. Phys. Conf. Ser. 1561 (1) (Jun. 2020) 012008, https://doi.org/10.1088/1742-6596/1561/1/012008.